

**REDUCTIVE LEACHING OF LOW GRADE MANGANESE ORE  
USING BAMBOO SAW DUST**

by

SUHAINA ISMAIL

Thesis submitted in fulfillment of the requirements  
for the degree of  
Doctor of Philosophy

February 2014

## ACKNOWLEDGEMENTS

Bismillahirrahmanirrohim.

It would not have been possible to complete this research without the help and support of the kind people around me, to only some of whom it is possible to give particular mention here. Above all, first and foremost, I would like to thank Allah, who is all powerful. Thanks for the many blessing. You had bestowed on me especially in giving me the strength to complete my study.

I am grateful to my supervisor, Associate Professor Dr. Hashim Hussin and also my co-supervisor, Associate Professor Dr. Syed Fuad Saiyid Hashim for their vital role and patience, for being inspirational and for teaching me the importance of using curiosity as the driving force behind research. Without his advice and patience, this research would probably be unintelligible.

I wish to express my gratitude to my first supervisor, Dr. Zaimawati Zainol, who gave me the golden opportunity to do this wonderful research. I came to know about so many new things even though in one and half year with her.

I am also indebted to Dr. Norazharuddin Shah Abdullah for his invaluable lessons about the importance for guidance and the freedom he granted to me during my work in the lab and guidance from beginning to final level of my thesis writing. He was willing to take time to help me adding some new ideas to my research, the support and also has been invaluable on both academic and friendship, for which I am extremely grateful. Without his guidance and patience, I probably would not be able to complete my research and thesis writing. Thank you for teaching me how to become a researcher. May Allah bless you.

I also have a large debt to the School of Materials and Mineral Resources Engineering, Universiti Sains Malaysia especially to the Dean, the Deputy Dean and the management staff for all their help and support. Much appreciation is extended to the technical staff for their technical support and teaching me experimental techniques during my work in the lab. In particular, I wish to express my gratitude to Madam Fong Lee Lee, Madam Haslina, Mr.Rashid, Mr.Kemuridan and others.

I would also like to acknowledge USM for providing ASTS scholarship and Research University Postgraduate Research Grant Scheme for the financial support of this study.

Heartfelt gratitude goes to my beloved husband, Mohamad Hasnor bin Husin for his personal support and great patience at all time. My children, Haziq Mus'ad, Muhammad Hazim Muqri, Harraz Mursyid and Ainul Mardhiah who are always understanding and supportive. Thanks to parents, my late father, and mother. Both of you are always in my heart. Also to my in-law family, brother and sisters who have given me their unequivocal support throughout the years. To my close friends who have offered such precious emotional support that will never be forgotten. My thanks go especially to Dr. Hasmaliza, Norwanis, Siti Aida and Nurul Ain.

Last, but by no means least, I thank to those who are involved either directly concerning this research or indirectly in other aspect of my study. For any errors or inadequacies that may remain in this work, of course, the responsibility is entirely my own.

Thank you very much.

## TABLE OF CONTENTS

	<b>Page</b>
<b>ACKNOWLEDGEMENTS</b>	ii
<b>TABLE OF CONTENTS</b>	iv
<b>LIST OF TABLES</b>	xi
<b>LIST OF FIGURES</b>	xiv
<b>LIST OF ABBREVIATIONS</b>	xx
<b>LIST OF SYMBOLS</b>	xxii
<b>ABSTRAK</b>	xxv
<b>ABSTRACT</b>	xxvi
<b>CHAPTER ONE : INTRODUCTION</b>	
<b>1.1 Significant of research work</b>	1
<b>1.2 Problem statements</b>	5
<b>1.3 Objectives of the research</b>	7
<b>1.4 Scope of works</b>	7
<b>1.5 Thesis organization</b>	9
<b>CHAPTER TWO : LITERATURE REVIEW</b>	
<b>2.1 Introduction</b>	11
<b>2.2 The occurrence of Mn ore</b>	12
2.2.1 Mineralogical assemblages and element associations	13
2.2.1(a) Pyrolusite: Relationship to manganite and $Mn_5O_8$	14
2.2.1(b) Significant mineral in LGMO- Al-substituted Goethite ( $Fe_{0.93}Al_{0.07}$ ) OOH	17
2.2.2 Classification of manganese ore	19
2.2.3 Impurities in Mn ore	20
<b>2.3 Application of manganese ore</b>	21
<b>2.4 Production and consumption of Mn ores; steel production and, domestic price</b>	22

<b>2.5</b>	<b>Alternative resources of Mn ore</b>	25
<b>2.6</b>	<b>Mn reserves in Malaysia</b>	26
<b>2.7</b>	<b>Research work background on LGMO treatment</b>	28
2.7.1	Reductive leaching by organic reductant	29
2.7.2	Reductive leaching of low grade Mn ore using pure carbohydrate and industrial or agro-waste as reducing agent in H <sub>2</sub> SO <sub>4</sub> medium	30
<b>2.8</b>	<b>Thermodynamic of leaching reactions (Eh-pH diagram)</b>	35
2.8.1	The Mn-H <sub>2</sub> O-H <sub>2</sub> SO <sub>4</sub> system	36
<b>2.9</b>	<b>Leaching kinetics of low grade ores</b>	38
2.9.1	Rate of dissolution	39
2.9.2	Shrinking core model (SCM)	40
2.9.2(a)	Diffusion through gas film as rate limiting	40
2.9.2(b)	Diffusion through porous product layer as rate limiting	43
2.9.2(c)	Chemical reaction as rate limiting	45
2.9.3	Shrinking spherical particles	47
2.9.4	Variable activation energy model	49
2.9.5	Factors affecting manganese leaching kinetics	50
2.9.6	Factors affecting goethite leaching kinetics	57
<b>2.10</b>	<b>The bamboos of Peninsular Malaysia</b>	58
2.10.1	Structure of bamboo	59
2.10.2	Propagation and silviculture	61
2.10.3	Commercial application of various bamboo species	61
<b>2.11</b>	<b>Carbohydrates</b>	63
2.11.1	The nature of lignocellulose	63
2.11.1(a)	Cellulose	66
2.11.1(b)	Hemicellulose	67
2.11.1(c)	Lignin	69
2.11.2	Hydrolysis of cellulose	70
2.11.2(a)	Acid hydrolysis process	71

2.11.2(b) Enzyme hydrolysis process	73
2.11.2(c) Microbial hydrolysis processes	74

## **CHAPTER THREE : MATERIALS AND METHODS**

<b>3.1 Introduction</b>	75
<b>3.2 Materials</b>	75
3.2.1 Low grade manganese ore (LGMO) and Bamboo sawdust (BSD)	75
<b>3.3 Sample preparation of LGMO and BSD</b>	77
3.3.1 LGMO sample preparation	77
3.3.2 Ore visual assessment and ore morphological studies	79
3.3.3 Mineral liberation studies of LGMO	80
3.3.4 BSD sample preparation	80
<b>3.4 Sequential procedure of Response Surface Methodology (RSM) on statistical design</b>	81
3.4.1 Selection of process factor and construction of $2^3 + s$ factorial design	83
3.4.2 New region points by steepest ascent method	88
3.4.3 Central composite design (CCD) of RSM for optimal setting for Mn extraction	89
<b>3.5 Batch leaching experimental set up and procedure</b>	89
<b>3.6 Kinetic studies</b>	92
<b>3.7 Analytical analysis procedure</b>	92
3.7.1 Determination of moisture and ash content	92
3.7.2 Determination of extractives	93
3.7.3 Biomass constituent determination	95
3.7.3(a) Determination of acid-insoluble lignin (Klason lignin)	95
3.7.3(b) Determination of holo-cellulose, cellulose and hemicellulose	97

<b>3.8</b>	<b>Characterisation of LGMO and BSD</b>	100
3.8.1	Particle size analysis (PSA)	100
3.8.2	Elemental composition by X-ray fluorescence (XRF)	101
3.8.3	Mineral Phases Identification by XRD	101
	3.8.3(a) Sample preparation of LGMO	101
	3.8.3(b) Data Measurement	102
	3.8.3(c) Rietveld refinement	102
3.8.4	Crystallinity of BSD by XRD	103
3.8.5	Morphology of LGMO and BSD by FESEM	103
3.8.6	Spectroscopic characterization of BSD by FTIR	104
3.8.7	Determination of Mn in the presence of iron by EDTA titration	104
	3.8.7(a) Reagents and solutions	104
	3.8.7(b) Titration procedure	105
3.8.8	Determination of Fe and Al by Inductive Couple Plasma (ICP)	106
	3.8.8(a) Reagents and standards	106
	3.8.8(b) Instrumentations	106
	3.8.8(c) Operating conditions	104
	3.8.8(d) Sample preparations	107
	3.8.8(e) Standard Calibrations	108

## **CHAPTER FOUR : RESULTS AND DISCUSSION**

<b>4.1</b>	<b>Introduction</b>	109
<b>4.2</b>	<b>Visual assessment of Sungai Temau's LGMO</b>	110
<b>4.3</b>	<b>Morphological studies</b>	111
<b>4.4</b>	<b>Mineral distribution and liberation of LGMO</b>	115
<b>4.5</b>	<b>Characterisation of LGMO</b>	119
	4.5.1 Particle size analysis (PSA)	119
	4.5.2 Elemental composition analysis (XRF)	120

4.5.3	Mineral phases identification of LGMO	122
<b>4.6</b>	<b>BSD Characterization</b>	127
4.6.1	Particle size analysis (PSA)	128
4.6.2	Biomass Determination	129
4.6.3	Chemical composition of BSD from XRF analysis	131
4.6.4	Morphology of BSD	131
4.6.5	Crystallinity of BSD	133
4.6.6	Molecular framework of BSD (FTIR)	134
<b>4.7</b>	<b>A Sequential response surface method (RSM)</b>	136
4.7.1	Analysis of variance of factorial design	136
4.7.2	Verification of the first order model	143
	4.7.2(a) Mn extraction as a function of the leaching time	146
4.7.3	New region points by steepest ascent method	148
4.7.4	Central composite design (CCD) of RSM for optimal setting of Mn extraction	152
4.7.5	Verification of the second order model of CCD design	156
4.7.6	Relationship between Mn extractions with process variables of leaching	157
	4.7.6(a) Effect of temperature and H <sub>2</sub> SO <sub>4</sub> concentration	159
	4.7.6(b) Effect of temperature and bamboo mass	159
	4.7.6(c) Effect of H <sub>2</sub> SO <sub>4</sub> concentration and bamboo loading	160
	4.7.6(d) Mn extraction as a function of the leaching time	162
4.7.7	Multiple responses by overlay contour plot	165
4.7.8	Verification of second order model of Fe and Al	171
4.7.9	Relationship of Fe and Al dissolution with leaching process variable	173
	4.7.9(a) Effect of temperature and H <sub>2</sub> SO <sub>4</sub> concentration on Fe dissolution	173
	4.7.9(b) Effect of temperature and bamboo loading on Fe dissolution	175



4.7.9(c) Effect of H <sub>2</sub> SO <sub>4</sub> concentration and bamboo mass on Fe dissolution	175
4.7.9 (d) Effect of temperature and H <sub>2</sub> SO <sub>4</sub> concentration on Al dissolution	176
4.7.9 (e) Effect of temperature and bamboo loading on Al dissolution	176
4.7.9(f) Effect of H <sub>2</sub> SO <sub>4</sub> concentration and bamboo mass on Fe dissolution	176
4.7.10 Multiple responses by overlay contour plot	178
<b>4.8 Effect of BSD hydrolysis on Mn extraction</b>	181
<b>4.9 Kinetic modelling of LGMO in H<sub>2</sub>SO<sub>4</sub> solution</b>	187
4.9.1 Effect of temperature	192
<b>4.10 Characterisation of leached residue obtained from reductive H<sub>2</sub>SO<sub>4</sub> leaching of LGMO</b>	197
4.10.1 LGMO elemental composition analysis (XRF)	197
4.10.2 LGMO mineral phases	198
4.10.3 LGMO morphologies	200
4.10.4 BSD morphologies	202
4.10.5 Crystalline index of BSD	204
 <b>CHAPTER FIVE : CONCLUSION AND RECOMMENDATIONS</b>	
<b>5.1 Conclusion</b>	207
<b>5.2 Recommendations for future work</b>	210
 <b>REFERENCES</b>	212
 <b>APPENDICES:</b>	
<b>Appendix A</b>	228
<b>Appendix B</b>	229
<b>Appendix C</b>	231
<b>Appendix D</b>	236

<b>Appendix E</b>	238
<b>Appendix F</b>	139
<b>Appendix G</b>	249
<b>Appendix H</b>	260
<b>LIST OF PUBLICATION</b>	261

## LIST OF TABLES

	<b>Page</b>
Table 2.1: The most common modes of manganese with variable elemental composition and identification (Burke and Uytendogaardt, 1985).	14
Table 2.2: Unit cell dimensions of pyrolusite, manganite, and Mn <sub>5</sub> O <sub>8</sub> (Rask and Buseck, 1986)	16
Table 2.3: Summaries of world production of manganese ore, ferromanganese and silicomanganese and U.S manganese consumption between 2006 to 2010 (Corathers, 2008; 2009; 2010; 2011; 2012).	23
Table 2.4: Reductive leaching by organic reductants (Zhang and Cheng, 2007).	30
Table 2.5: Reductive leaching of low grade Mn ore using pure carbohydrate	32
Table 2.6: Reductive leaching of low grade Mn ore using industrial or agro-waste as reducing agent in H <sub>2</sub> SO <sub>4</sub> medium.	33
Table 2.7: Activation energy value for predicting reaction control.	49
Table 2.8: Previous research on the leaching kinetics of pyrolusite or MnO <sub>2</sub> .	51
Table 2.9: Cellulose, hemicellulose, and lignin contents in common agricultural residues and wastes (Kumar, et al., 2009).	64
Table 3.1: Control factor and their levels in the reductive Mn leaching experiments.	84
Table 3.2: Experimental runs of 2 <sup>3</sup> +s factorial design for reductive leaching of Mn.	84
Table 3.3: New control factor and their levels in the reductive Mn leaching experiments.	87
Table 3.4: New factorial design for second first order model.	87
Table 3.5: CCD for second order model.	89
Table 3.6: Optima 7300 DV Operating Conditions.	107
Table 3.7: Standard solution concentration range for ICP.	108

Table 4.1:	Semi-quantitative elemental composition of LGMO at different size fraction.	121
Table 4.2:	Biomass constituent of BSD and other biomass resources on dry weight basis (wt %).	130
Table 4.3:	Elemental composition of BSD.	131
Table 4.4:	Infrared Transmittance Peaks ( $\text{cm}^{-1}$ ) of BSD and other biomass resources.	135
Table 4.5:	Result of $2^3 + s$ factorial design: Process data for fitting the first-order model.	138
Table 4.6:	ANOVA for the first order model.	138
Table 4.7:	Estimated effects and coefficients for Mn extraction.	139
Table 4.8:	Residual analysis summary of factorial design.	143
Table 4.9:	Steepest ascent experiment.	148
Table 4.10:	New control factor and their levels in the reductive Mn leaching experiments.	149
Table 4.11:	New factorial design and results for fitting of second first order model.	150
Table 4.12:	Analysis of variances (ANOVA) for the second first order model.	150
Table 4.13:	Estimated effects and coefficients for Mn extraction	151
Table 4.14:	Experimental design matrix of CCD and corresponding response.	152
Table 4.15:	Analysis of variances (ANOVA) for the second order model.	153
Table 4.16:	Estimated regression coefficients for Mn extraction.	153
Table 4.17:	Residual analysis summary of CCD design.	154
Table 4.18:	Optimum conditions of reductive leaching by natural carbohydrate as reducing agent.	158
Table 4.19:	Experimental design matrix of CCD and corresponding response (Fe and Al dissolution).	166
Table 4.20:	Analysis of variance (ANOVA) and estimated regression coefficient for Fe and Al dissolution.	167

Table 4.21:	Residual analysis summary of Fe and Al dissolution.	171
Table 4.22:	Verification experiments in the optimum area.	179
Table 4.23:	Experimental plan, Mn extraction and apparent dissolution rate in sulphuric leaching.	191

## LIST OF FIGURES

	<b>Page</b>
Figure 2.1: A drawing to illustrate the dimension of the pyrolusite, manganite, and $Mn_5O_8$ unit cell and their relative orientations in the topotactic reactions (Rask and Buseck, 1986).	15
Figure 2.2: Potential-pH diagram for Mn-H <sub>2</sub> O-H <sub>2</sub> SO <sub>4</sub> system (Kelsall, 2000).	36
Figure 2.3: Basic sketch of leaching dissolution process (Biomine, 2006).	39
Figure 2.4: The cross section of partly reacted solid particles, unreacted solid material surrounded by a layer of ash.	40
Figure 2.5: Representation of a reacting particle when chemical reaction is the controlling resistance (Levenspiel, 1999).	43
Figure 2.6: Representation of a reacting particle when diffusion through the product layer in the controlling resistance (Levenspiel, 1999).	46
Figure 2.7: Representation product for the reaction $A(aq.) + bB(s) \rightarrow rR(g)$ between a shrinking solid particle and liquid.	48
Figure 2.8: Cum nodes and internodes; (a) intermodal segment with two nodes; (b) diagram of transverse section of culm showing thick walled culm and solid culm; (c) longitudinal section through a node, showing the septum or cross wall (Wong, 1995).	60
Figure 2.9: Lignocellulose and its components; cellulose, hemicellulose and lignin (Lignocellulosic biomass, 2006).	65
Figure 2.10: The partial molecular structure of cellulose, 1,4- $\beta$ -glycoside bond ( $\beta$ -D-glucopyranoside) polymer (McMurry, 2008).	66
Figure 2.11: Interconversion of the polymorphs of cellulose (O'Sullivan, 1996).	67
Figure 2.12: Monomer components of wood hemicelluloses.	68

Figure 2.13:	The three primary lignin monomers M, monolignols p-coumaryl alcohol M <sub>H</sub> , coniferyl alcohol M <sub>G</sub> , and sinapyl alcohol M <sub>S</sub> and lignin structural p-hydroxyphenyl, guaiacyl, and syringyl units P <sub>H</sub> , P <sub>G</sub> , and P <sub>S</sub> , derived from them through free radical coupling reactions.	69
Figure 3.1:	A flowchart representing an overall experimental work.	76
Figure 3.2:	A flowchart illustrating a sample preparation procedure of LGMO and BSD.	78
Figure 3.3:	Sequential procedure of RSM on statistical design a) Selection of process variables; b) Seeking a new region points; c) Construction of CCD.	82
Figure 3.4:	Path of steepest ascent (Minitab, Technical Support Document).	86
Figure 3.5:	A schematic diagram of a) Reductive leaching set-up; b) Soxhlet extraction set-up	91
Figure 3.6:	A flowchart displaying an extractive determination procedure.	94
Figure 3.7:	A flowchart displaying acid-insoluble lignin determination procedure.	96
Figure 3.8:	A flowchart displaying holocellulose, cellulose and hemicellulose determination procedure.	99
Figure 4.1:	Irregular shape of LGMO with varying colour (light gray to brownish); (black and white elongated crystal) originated in argillized rock from Sungai Temau, Pahang iron ore site.	110
Figure 4.2:	Optical microscope micrograph showing the complexity of mineralogy and texture of LGMO. Total magnification=3958X, (a) Zoning structure of Mn phases and Quartz (b) Disseminated Mn phases in quartz gangue.	111
Figure 4.3:	BSI photomicrograph of (a) Very fine Mn phase intergrowth in Si phase, (b) fibrous Mn phase contained aluminium-iron phases, (c) zoning structure of different grey level of Mn phase and aluminium-iron phases.	112
Figure 4.4:	BSI photomicrograph of EDX line scan showing compositional variation.	114

Figure 4.5:	BSI of nine sample micrographs to distinguish the degree of mineral liberation at different LGMO size fractions.	116
Figure 4.6:	Comparison of SEM image and ImageJ image; a) original image before threshold, b) threshold image from Image J analysis system.	117
Figure 4.7:	Resulting data from image analysis of the particle in Figure 4.5 (f-i), shown as a percentage of the mineral liberation at particle size fraction of (-350+250) $\mu\text{m}$ , (-250+150) $\mu\text{m}$ , (-150+75) $\mu\text{m}$ , and -75 $\mu\text{m}$ .	118
Figure 4. 8:	a) Backscattered electron image and b) Elemental x-ray mapping c) The green region of the particle is identified as pyrolusite and d) The yellow region is identified as goethite.	119
Figure 4.9:	PSD of ground LGMO $\leq 75\mu\text{m}$ ; cumulative and volume distribution curves.	120
Figure 4.10:	XRD pattern of LGMO samples. Abbreviation: Q, Quartz; P,Pyrolusite; G, Aluminium- Goethite.	123
Figure 4.11:	Comparison of observed XRD pattern (top), calculated pattern (middle) and difference pattern between them for LGMO samples.	126
Figure 4.12:	a) The average size of bamboo received (80 x 5x 40) mm; b) The bamboo was preliminary reduced by cutting mill to achieve (5 x 5 x 40) mm; c) Bamboo chip were then shredded into fines ( $\leq 250$ )	127
Figure 4.13:	PSD of ground BSD < 250 $\mu\text{m}$ ; cumulative and normal distribution curves.	128
Figure 4.14:	a) SEM morphology of BSD, needle like shape with multiple well aligned bundles; b) fibrils structure; c) rigidity of cell wall d) EDX analysis of BSD at whole area of image 4.14c.	132
Figure 4.15:	X-ray diffraction patterns of the BSD with major crystal planes of cellulose labelled with solid arrows, dotted arrow depicts amorphous region.	134
Figure 4.16:	FT-IR spectra of BSD indicate molecular framework of cellulose and hemi-cellulose structure.	135
Figure 4.17:	Experimental vs. predicted data for Mn extraction.	140



Figure 4.18:	Residual analysis a) Normal probability plot; b) Standardized normal probability plot; c) Residual vs. Fitted value; d) Residual vs. Run order; e) Residual vs. Factor (H <sub>2</sub> SO <sub>4</sub> concentration); f) Residual vs. Factor (Temperature).	142
Figure 4.19:	Main effect plot for each level on Mn extraction.	144
Figure 4.20:	Interaction plot of H <sub>2</sub> SO <sub>4</sub> and temperature on Mn extraction.	145
Figure 4.21:	The three-dimensional response surface and contour plot of Mn extraction as a function of temperature (X <sub>1</sub> ) and H <sub>2</sub> SO <sub>4</sub> concentration (X <sub>2</sub> ).	146
Figure 4.22:	H <sub>2</sub> SO <sub>4</sub> concentration and temperature effect on the leaching process; 8g bamboo, 10% (w/v) pulp density.	147
Figure 4.22:	Mn extraction steps along the path of steepest ascent.	149
Figure 4.23:	Residual analysis of second order model a) Normal probability plot; b) Histogram c) Residual vs. Fitted value; d) Residual vs. Run order; e) Residual vs. Factor (Temperature) f) Residual vs. Factor (H <sub>2</sub> SO <sub>4</sub> ); g) Residual vs. Factor (bamboo loading).	155
Figure 4.25:	Scatter diagram of experimental Mn extraction vs. predicted Mn extraction.	157
Figure 4.26:	Response surface and contour plot of the illustrating a surface with a maximum; a) Mn extraction as a function of temperature (X <sub>1</sub> ) and H <sub>2</sub> SO <sub>4</sub> concentration (X <sub>2</sub> ); b) Mn extraction as a function of temperature (X <sub>1</sub> ) and bamboo loading (X <sub>3</sub> ); c) Mn extraction as a function of H <sub>2</sub> SO <sub>4</sub> concentration (X <sub>2</sub> ) and bamboo loading (X <sub>3</sub> ).	161
Figure 4.27:	Manganese extraction curves vs. time; <i>Size of ore: ≤75 μm, duration of leach: 8 hours (480 minutes), pulp density: 10%; *Average value of run 9, 10 and 11 (see Table 4.12).</i>	162
Figure 4.28:	Residual analysis of Fe dissolution a) Normal probability plot; b) standardized residual plot; c) Residual vs. Fitted value; d) Residual vs. Run order; e) Residual vs. Factor (Temperature) f) Residual vs. Factor (H <sub>2</sub> SO <sub>4</sub> ); g) Residual vs. Factor (bamboo loading).	168

Figure 4.29:	Residual analysis of Al dissolution a) Normal probability plot; b) Standardized residual plot; c) Residual vs. Fitted value; d) Residual vs. Run order; e) Residual vs. Factor (Temperature) f) Residual vs. Factor (H <sub>2</sub> SO <sub>4</sub> ); g) Residual vs. Factor (bamboo loading)	170
Figure 4.30:	Scatter diagram of a) predicted values for Fe dissolution; b) predicted values for Al dissolution.	172
Figure 4.31:	Response surface and contour plot (illustrating a surface with a minimum); a) Fe dissolution as a function of temperature (X <sub>1</sub> ) and H <sub>2</sub> SO <sub>4</sub> concentration (X <sub>2</sub> ); b) Fe dissolution as a function of temperature (X <sub>1</sub> ) and bamboo loading (X <sub>3</sub> ); c) Fe dissolution as a function of H <sub>2</sub> SO <sub>4</sub> concentration (X <sub>2</sub> ) and bamboo loading (X <sub>3</sub> ).	174
Figure 4.32:	Response surface and contour plot of the illustrating a surface with a minimum; a) Al dissolution as a function of temperature (X <sub>1</sub> ) and H <sub>2</sub> SO <sub>4</sub> concentration (X <sub>2</sub> ); b) Al dissolution as a function of temperature (X <sub>1</sub> ) and bamboo loading (X <sub>3</sub> ); c) Al dissolution as a function of H <sub>2</sub> SO <sub>4</sub> concentration (X <sub>2</sub> ) and bamboo loading (X <sub>3</sub> ).	177
Figure 4.33:	Overlaid contour plots of combined responses (Mn extraction, Fe and Al dissolution); a) function of temperature (X <sub>1</sub> ) and H <sub>2</sub> SO <sub>4</sub> concentration (X <sub>2</sub> ); b) function of temperature (X <sub>1</sub> ) and bamboo loading (X <sub>3</sub> ); c) function of H <sub>2</sub> SO <sub>4</sub> concentration (X <sub>2</sub> ) and bamboo loading (X <sub>3</sub> )	179
Figure 4.34:	Relationship of Mn extraction and BSD constituent during leaching test at temperature, 90°C, [H <sub>2</sub> SO <sub>4</sub> ], 2M; BSD amount, 7.5g.	183
Figure 4.35:	Mechanisms of hydrolysis of cellulose in acidic (H <sup>+</sup> ) (Tanksale, et al., 2010).	184
Figure 4.36:	Kinetic model applied to the LGMO reductive leaching results (Experiment 15).	190
Figure 4.37:	Effect of temperature on Mn extraction, [H <sub>2</sub> SO <sub>4</sub> ], 2M; BSD amount, 7.5g.	193
Figure 4.38:	Plot of $1 - \frac{2}{3}X - (1 - X)^{2/3}$ vs. time for different reaction temperature.	194
Figure 4.39:	Plot of $\frac{1}{3}\ln(1 - X) + [(1 - X^{-1/3} - 1)]$ vs. time for different reaction temperature.	195

Figure 4.40:	Arrhenius plot for LGMO leaching at (2M H <sub>2</sub> SO <sub>4</sub> and 7.5g BSD loading).	196
Figure 4.41:	Semi-quantitative elemental composition of leached residue at different reaction time.	197
Figure 4.42:	XRD pattern of LGMO (a) before and (b) after reductive leaching; Q, Quartz; P, Pyrolusite; G, Aluminium- Goethite.	199
Figure 4.43:	SEM and EDX analysis of the ore (a) before leaching and (b) after 2 hours leaching time; (c) after 4 hours leaching time.	201
Figure 4.44:	SEM images of BSD: a & b; BSD before reductive leaching in H <sub>2</sub> SO <sub>4</sub> at different magnifications; c, d, e, f, g & h; BSD after leaching in H <sub>2</sub> SO <sub>4</sub> .	203
Figure 4.45:	X-ray diffraction pattern of BSD after leaching in 2M H <sub>2</sub> SO <sub>4</sub> by 7.5g BSD at 90°C.	205
Figure 4.46:	Crystallinity of BSD as a function of leaching duration time.	206

## LIST OF ABBREVIATION

ANOVA	Analysis of Variance
BSD	Bamboo Saw Dust
BSE	Back-scattered Electron
BSI	Back-scattered Image
CCD	Central Composite Design
CCV	Continuing Calibration Verification
CMD	Chemical Manganese Dioxide
DF	Degree of Freedom
DOE	Design of Experiment
EDTA	Ethylenediaminetetraacetic Acid
EDX	Energy Dispersive X-Ray
EMD	Electrolytic Manganese Dioxide
F	Fisher Test
FESEM	Field Emission Scanning Electron Microscopy
FRIM	Forest Research Institute Malaysia
FTIR	Fourier Transform Infrared Spectroscopy
HMF	Hydroxyl Methyl Furfuraldehyde
ICP	Inductively Coupled Plasma
ICSD	Inorganic Crystal Structure Database
IDL	Instrument Detection Limits
LGMO	Low Grade Manganese Ore
MDL	Method Detection Limits
Mt	Metric Ton
Mtu	Metric Ton Per Unit
ODW	Oven Dry Weight

P	Hypothesis
PPM	Parts Per Million
PSA	Particle Size Analysis
PSD	Particle Size Distribution
$R^2$	Correlation coefficient
RCS	Rate Controlling Step
RF	Radio Frequency
RSD	Relative Standard Deviation
RSM	Response Surface Methodology
SCD	Segmented Array Charge Coupled Detector
SCM	Shrinking Core Model
SEM	Scanning Electron Microscopy
SS	Sum Of Square
VMD	Volume Moment Diameter
$W_F$	Final Weight
$W_I$	Initial Weight
XRD	X-Ray Diffraction Spectroscopy
XRF	X-Ray Fluorescence

## LIST OF SYMBOLS

%	Percentage
<	Less than
>	More than
°C	Degree celsius
°C/min	Degree Celsius per minute
[ ]	Concentration
μm	Micrometer
$\xi'_s$	Natural variables
$X'_s$	Coded variables
$y$	Response
$\beta$ 's	Parameters whose values are to be determined
$X$ 's	Variable that represent factor
$\varepsilon$	Random error
$Q_A$	Flux Of A Within The Ash Layer
$D$	Effective Diffusion Coefficient
$k''$	First Order Rate Constant For The Surface Reaction
$E$	Energy
$E_a$	Activation Energy
$k$	Reaction Rate
$A$	Frequency Factor Or Arrhenius Constant
$R$	Gas Constant
$C_x$	Concentration Of Cellulose
$C_l$	Concentration Of Glucose
$C_o$	Concentration Of Decomposed Glucose
$Y_1$ & $Y_2$	Stoichiometric Coefficients

$H_0$	Null Hypothesis
$t$	Time
$\tau$	Time required for the complete conversion of the $MnO_2$
$V$	Volume of particles
$B$	Solid particle B
$R$	Radius of solid particle B
$r_c$	Radius of unreacted core
$C_{Ag}$	Concentration of A at the gas film
$C_{As}$	Concentration of A at the particle surface
$C_{Ac}$	Concentration of A at the unreacted core surface
$C_{A0}$	Initial acid concentration in the selected test (M)
$C_{LO}$	Initial lactose concentration in the selected test (M)
$C'_{AS}$	Stoichiometric sulphuric acid requirement
$C'_{LS}$	Stoichiometric glucose requirement
$C_H$	Reaction order of $H_2SO_4$
$C_W$	Reaction order of MSW
$S_{ex}$	Unchanging exterior surface of particle
$\rho_B$	Molar density of B
$k_g$	Mass transfer coefficient between fluid and particle
$X_B$	Fractional conversion of solid B
$N_B$	Mole of solid B
$N_A$	Mole of reactant A
$K_c$	Chemical reaction rate constant
$K_d$	Diffusion reaction rate constant
$M_B$	Molecular weight of solid
$\alpha$	Stoichiometric Coefficient

$R_{wp}$	R weight profile
$R_{exp}$	R expected
$R_p$	Particle size
$T'$	Reference temperature
$\chi^2$	Goodness of fit



# PELARUT LESAPAN PENURUNAN BIJIH MANGAN BERGRED RENDAH DENGAN MENGGUNAKAN HABUK BULUH

## ABSTRAK

Pengekstrakan mangan (Mn) daripada bijih Mn yang bergred rendah (LGMO) melalui proses pelarut lesapan penurunan telah dikaji di dalam penyelidikan ini. Proses pelarutlesapan penurunan ini telah dijalankan dalam medium berasid ( $H_2SO_4$ ), dengan menggunakan habuk buluh (BSD) sebagai agen penurunan. Pencirian fasa mineral ke atas LGMO menunjukkan ianya terdiri daripada fasa pirolusit,  $\alpha$ -kuarza dan goethite. Sementara itu, komposisi biojisim BSD yang digunakan mengandungi 38.96% selulosa, 26.95% hemiselulosa dan 25.86% lignin. Dalam menentukan pengekstrakan Mn secara optimum, rekabentuk eksperimen melalui kaedah maklumbalas permukaan (RSM) berturutan telah dilaksanakan. Didapati pemboleh ubah yang paling ketara ke atas pelarutlesapan LGMO ialah suhu diikuti dengan kepekatan  $H_2SO_4$  dan jisim BSD. Pengekstrakan Mn yang melebihi 95% dengan pelarutan yang rendah bagi Fe (<30%) dan Al (<10%) telah dicapai apabila suhu proses pelarutresapan berada dalam julat  $90^\circ C \leq T \leq 110^\circ C$ ; dengan julat kepekatan  $H_2SO_4$   $1.5M \leq H_2SO_4 \leq 2.5M$  dan jisim BSD sebanyak 7.5g. Kinetik tindak balas bagi proses pelarutlesapan ini telah ditentukan dan didapati sepadan dengan model  $1 - \frac{2}{3}X - (1 - X)^{\frac{2}{3}} = K_d$  dengan nilai  $E_a$  sebanyak 69.3kJ/mol. Kadar tindak balas bagi proses pelarut lesapan LGMO dengan menggunakan BSD terkawal secara pembauran melalui lapisan lengai. Pencirian ke atas sisa LGMO terlarutlesap menunjukkan bahawa komponen asid larut telah terlarut semasa proses pelarutlesapan, dengan selulosa dan hemiselulosa dalam sisa BSD telah terurai. Oleh itu, kesimpulannya habuk buluh (BSD) boleh digunakan sebagai agen penurunan alternatif dalam pengekstrakan Mn daripada bijih mangan yang bergred rendah.

## REDUCTIVE LEACHING OF LOW GRADE MANGANESE ORE USING BAMBOO SAWDUST

### ABSTRACT

Extraction of manganese (Mn) from low grade manganese ore (LGMO) through reductive leaching was studied in this research work. The reductive leaching process was done in acidic medium ( $H_2SO_4$ ) and bamboo sawdust (BSD) was used as reducing agent. Mineral phase characterization on LGMO showed that the ore consist of phases of pyrolusite,  $\alpha$ -quartz and goethite. Meanwhile, the biomass composition of BSD used in this work contains 38.96% cellulose, 26.95% hemicellulose and 25.86% lignin. In determination of optimum Mn recovery, design of experiment through a sequenced response surface method (RSM) was done. It was observed that the most significant variable on the leaching of LGMO is temperature, followed by concentration of  $H_2SO_4$  and mass of BSD. Extraction of Mn above 95% with low dissolutions of Fe (<30%) and Al (<10%) was achieved at leaching temperature between the range of  $90^\circ C \leq T \leq 110^\circ C$ ;  $H_2SO_4$  concentration of  $1.5M \leq H_2SO_4 \leq 2.5M$  and BSD mass of 7.5g. The reaction kinetics of this leaching process was determined, and it was observed to fit the model of  $1 - \frac{2}{3}X - (1 - X)^{\frac{2}{3}} = K_d t$  with  $E_a$  of 69.3kJ/mol. The reaction rate for LGMO leaching using BSD was found to be diffusion through inert layer. Characterization on LGMO leach residue showed that are acid soluble component were dissolved during the leaching, with cellulose and hemicellulose in BSD residue were ravelled. Hence, it can be concluded that bamboo saw dust (BSD) can be used as an alternative reducing agent in the extraction of Mn from low grade manganese ore.

## CHAPTER 1

### INTRODUCTION

#### 1.1 Significant of research work

Low grade manganese ore (LGMO) has received much attention in recent years due to the increase in demand of the world's high grade manganese (Mn) ores particularly in steel production. As a number of products from Mn applications continue to rise, the Mn demand continues to increase. However, the metal's supply remains limited. With the ever demand supply of valuable elements, the task of recovery of Mn from LGMO becomes significant. Due to that, some deposits, which were previously considered low grade, are now economically mined (Leja and Qazi, 1971; Azzam and Abd El Rahim, 1985; El Tawil, et al., 1989; El Hazek, et al., 2006).

LGMO have a complicated mineralogical constituent which are generally made up of intergrowth minerals, often with interlocked and finely disseminated metal oxides. Furthermore it is associated with different grade of metamorphic rock with complicated structural (i.e., crystallographic intergrowth and replacement texture) (Roy, 1981). Different minerals from different locations have different mineralogical composition with different characteristics and complexities. Enrichment of low grade ores, however, is not trivial. The understanding of mineralogical, chemical composition, size, morphology and association with other minerals are expected to paint a clear picture of the mineral's behaviour during the beneficiation and recovery processes (Olubambi, et al., 2008a).

Many processes have been investigated for the recovery of Mn from LGMO including pyro-hydrometallurgy or pure hydrometallurgy treatment using different kinds of lixiviant and reducing agent. Established methods of pyro-hydrometallurgy treatment in industries are sulphation roasting and reduction roasting (Zhang and Cheng, 2007). During sulphating roasting, sulphuric acid or ammonium sulphate are used as reducing agent and this step able to alter the Mn minerals ( $\text{MnO}_2$ ) to soluble sulphates. Then, the process is followed by water leaching. Meanwhile, high temperature ( $700\text{-}900^\circ\text{C}$ ) of reduction roasting was applied in order to convert higher valence manganese oxides ( $\text{MnO}_2$ ) to lower ones ( $\text{MnO}$ ) which are readily soluble in sulphuric acid. Maximum efficiency ( $>95\%$ ) in the recovery of Mn for both process can be achieved; however it requires more energy consumption.

An alternative treatment of LGMO with high efficient recovery of Mn is by direct reductive leaching. As reviewed by Zhang and Cheng (2007), the typical lixiviant in reductive leaching is hydrochloric acid, sulphuric acid and nitric acid. Numerous reducing agents were used in this treatment such as ferrous solution, sulfur dioxide solution, organic reductant, hydrogen peroxide, sulphide minerals and biology reductants (microorganism). Few researchers have addressed the use of organic reductants in the LGMO leaching process. Organic reductants are considered as non-hazardous, and well-known as low-cost reducing agents which able to be used under mild acidic condition. From the previous work done by the researchers, a great concern on classifying organic reductant has been highlighted. It can be divided into three types; organic acids and alcohol, sugar in pure form and agro-industrial waste. These different types of organic reductant used in the reductive leaching will give a different reaction and pathway of process. It will generate a different reaction by

product and affect the optimal condition of Mn recovery. In order to enhance the Mn recovery from LGMO, it is imperative to understand the characteristic and behaviour of organic reductant used in the leaching process.

Amongst the organic acid and alcohol used as reductant are oxalic acids and methanol. For examples, Sahoo, et al. (2001) showed that 98% of Mn extraction with low iron dissolution was achieved by using oxalic acid and Momade (1999) established the optimum conditions of Mn extraction. However, although the ability of oxalic acid and methanol to reduce metals from higher to lower oxidation state was demonstrated, little attention has been paid to the high requirement of temperature during the leaching process.

It has been found that several work have been focused on pure formed of sugar such as glucose (Trifoni, et al., 2000; Trifoni, et al., 2001; Pagnanelli, et al., 2004; Furlani, et al., 2009), sucrose (Veglio and Toro, 1994a; Veglio and Toro, 1994b; Beolchini, et al., 2001) and lactose (Veglio, et al., 2000; Veglio, et al., 2001). The findings indicate a Mn recovery of up to 95% with low iron dissolution. However, the existence of different reaction pathways of glucose derivatives during leaching process has been found largely influence to the efficiency of Mn recovery.

The utilization of agricultural or industrial waste as reductant has generated considerable recent research interest. The application of the waste as potential reductant has been investigated by several researcher with high Mn recovery (over 90% with short reaction time in mild acidic condition); Adel, et al., 2004; Hariprasad, et al., 2007; Hariprasad, et al., 2009; Lasheen, et al., 2009; Su, et al.,

2009; Su, et al., 2010; Tian, et al., 2010; Yi-Ju, et al., 2011 and Yang, et al., 2013. In their work, the importance of chemical composition of agro-industrial waste is not well addressed. Chemical composition varies with type of carbohydrate, location and source. Thus, different reaction pathway and oxidative product will affect the Mn recovery.

Worldwide, 140 billion metric tons of biomass produced every year from agriculture. Biomass wastes include agricultural wastes which are normally produced through various farming activities. The generated biomass includes sugarcane leavings, poultry, straw, corn stalks, bagas, nutshells, forestry residues, such as wood chips, sawdust, mill scrap, timber, and bark; municipal waste, such as waste paper and yard clippings (United Nations Environmental Programme, 2009). When biomass at industrial-scale is discharged to the environment, it can have an impact on the environment. Therefore, the generated volume of biomass can be transformed to an enormous amount of energy and raw materials e.g., cordage, textiles, paper products, packaging materials, animal feed, insulators and panel boards. In fact, biomass is a renewable resource that has a steady and abundant supply. According to United Nations Environmental Programme (2009) report, approximately 50 billion tons of agricultural biomass waste can be converted to energy, which can substantially displace fossil fuel, reduce emissions of greenhouse gases and provide renewable energy. The utilization of biomass introduced ecological solid waste management, reduction of greenhouse gases, maximum utilization of resources, and promote energy efficient as well as environmental friendly technologies.

## 1.2 Problem statements

According to geological surveys by ECER (2012), a significant manganese ore deposits in Malaysia are located in states of Pahang and Kelantan. The ore produced by these mining activities is considered high of quality Mn, where it had high content of Mn 34% and low content of Fe 11.08%. However, from 115,000 mt per annum production capacities in 2008, approximately 60 % of this ore production produced were exported and while the remainder is used as one of the main raw materials to process silicomanganese alloy in Malaysia. This product was produced by manganese smelting plant owned by the Ratusan Ardi associate company, Eastcoast Universe Smelting & Mining (M) Sdn. Bhd (Ratusan Ardi, 2012). Concern with the Mn supply in the forthcoming year and the depletion of high grade Mn-ores, justify the studies on extractive process of low grade ores.

As mentioned earlier, LGMO are however, complicated mineralogical associations of constituent minerals. Owing to the complexities in the associated minerals of LGMO led to poor results on classification and characterization of the minerals (Hope, et al., 2001; Lane, et al., 2008; Olubambi, et al., 2008a). This is also influence the process flow for recovering/enrichment of constituent metals. For this reason, a comprehensive characterization method including mineral liberation studies could be adopted. This information will assist in the understanding of manganese recovery process, and its potential as a new resource for heavy mineral in Malaysia (after adequate enrichment).

Among the agricultural biomass produced in Malaysia, bamboo has a great potential as a natural resource feed stock in converting biomass into materials, e.g.,

reducing agent in sulphuric acid leaching. In fact, biomass is a renewable resource that has a steady and abundant supply that had been recognized as the second importance non-timber forest produced by the government in Malaysia next to rattan (Mohamad and Haron, 1990). However, detailed characteristics of carbohydrate sources were not sufficiently discussed especially for leaching applications. One way to promote the utilization of bamboo sawdust (BSD) carbohydrates is by proper understanding of its chemical constituents and chemical structure.

The strategy of experiment extensively practice is one factor-at-a-time approach. The disadvantages of this approach, is that fails to consider any possible interaction between the factors involves in the leaching process. A deeper understanding of biomass degradation and low grade manganese dissolution is needed in order to achieve a better comprehension and control of the leaching process. One solution to this problem is through design of experiments, because the results and conclusion that can be drawn from experiment depend to a large extent on the manner in which the data were collected. The data and understanding will facilitate the development of plant scale.

Despite the encouraging incentives from design of experiment as an alternative to typical experiment design for Mn recovery, there are still great challenges to be overcome. The BSD hydrolysis is dependent on chemical constituent of biomass which varies with tree part (root, stem or branch), type of wood, geographic location, climate and soil condition. Then, the dissolution reaction of low grade manganese is dependent on mineral composition.



### **1.3 Objectives of the research**

The main objectives of this research work are:

1. To characterize Sungai Temau's low grade manganese ore (LGMO).
2. To evaluate bamboo sawdust (BSD) as possible reducing agent.
3. To suggest an optimized acid leaching protocol (batch system) through statistical design method to extract Mn from LGMO with BSD as the reducing agent.
4. To propose the kinetics for Mn extraction from LGMO through acid leaching
5. To characterize a selected leach residues to support the findings in (3) and (4).

### **1.4 Scope of work**

The aim of this research is to characterize local LGMO, which is located at Sungai Temau, Pahang (in the east coast of peninsular Malaysia). The LGMO characterization is aided by X-ray fluorescence (XRF), X-ray diffraction (XRD), and Scanning electron microscopy (SEM) fitted with an Energy-dispersive x-ray analyzer (EDX) to determine elemental compositions, phase identification, and morphological conditions. This information will assist in the understanding of Mn recovery process, and its potential as a new resource for heavy mineral in Malaysia.

Furthermore, the aim of this research is to characterize bamboo sawdust (BSD) to be used as a carbohydrate source in leaching application. Characterization is conducted using Malvern analyzer (for particle size distribution, PSD), XRD (crystallinity), SEM (morphology) and FTIR spectrometer (molecular framework). Results for these analyses will provide a sound understanding of the possibility to use BSD as a reducing agent in the leaching of local LGMO. In this study, statistically

designed experiments were performed to investigate the Mn recovery from LGMO in sulphuric acid leaching using BSD as reductant.

A sequential response surface method (RSM) approach was used for optimizing the Mn extraction. In order to determine the most significant and interaction among operating factors (reaction temperature, sulphuric acid concentration and BSD loading) a  $2^{3+}$  factorial design was adopted and the experimental result (maximizing Mn extraction) were validated by the analysis of variance (ANOVA). The first order model (e.g., linear model) obtained was used to seek a region around the global optimum settings by the steepest ascend methods. Then, the optimization of leaching experiment using central composite design (CCD) was carried out and the adequacy of second order model obtained (e.g., quadratic model) was checked. In order to determine the quality of the leaching process, the Fe and Al dissolution have been monitored during the process. The responses simultaneously were considered by applying the overlay contour plot that visually identified as an area of compromise among the various responses (Maximizing Mn extraction and minimizing Fe and Al dissolution).

This work also considers the kinetic aspects of Mn leaching and the identification a kinetic model was examined and the apparent activation energy is determined. This model might be considered in the development of an overall kinetic model for LGMO reductive leaching using BSD.

## **1.5 Thesis organization**

This thesis is organised into five main chapters. Chapter one establishes the importance of Mn extraction from LGMO as a new resource for Mn ore. General background information regarding on Mn demand world view and complexity of LGMO mineralogy are described. Then, a brief overview of LGMO treatment process for the extraction of Mn from LGMO from previous and current research work are highlighted. Next, problem statements regarding this work were addressed and measurable objectives are described following with scope of work.

The most relevant part of the extensive literature on the subject is reviewed in Chapter two. This includes general background on Mn mineralogy, world production and demand of Mn, treatment process of LGMO, basic principles of mathematical modelling in regard to kinetic studies including some information on bamboo saw dust (BSD) as the chosen reductant in the reductive leaching of Mn.

Chapter three introduces the approaches and methodology used in this thesis as part of the research, such as sample preparation of LGMO and BSD, experimental strategy using sequential procedures of response surface methodology (RSM), experimental setup of reductive leaching and characterisation method of LGMO and BSD.

Full results analysis and discussion are presented in subsequent Chapter four. The section starts with the discussion of morphological and mineral liberation analysis of LGMO. Then, a subsequent section is dealt with the characterisation results of LGMO and BSD. The Mn extraction result which was analyzed by

ANOVA was described in detailed and the optimized leaching conditioned was discussed. The reaction rate and activation energy obtained from mathematical modelling of leaching process were discussed thoroughly. Finally, the discussion on leached liquor and solid residue characterization were presented as well.

The thesis is concluded in chapter five which contains the finding of current studies and recommendations for future work.

## CHAPTER 2

### LITERATURE REVIEW

#### 2.1 Introduction

This chapter aims to present a concise literature review on work relating to the extraction of manganese (Mn) from low grade manganese ore (LGMO). It starts with the Mn and all its trivial stuff such as occurrence, mineralogical assemblages and element associations, classification of Mn ore, the uses of Mn ore and the alternative resources of Mn ore. Considerable attention has also been given on world production of Mn ores, demand, and consumption of Mn. Then, in order to make use the local low grade source of Malaysian ore in this work, the history and current of mining deposited as well as mining activity in Malaysia were slightly reviewed. Many processes have been proposed for the treatment of LGMO, particularly on pyrometallurgy, pyro-hydrometallurgy and hydrometallurgy. However in this work, the hydrometallurgy approach was used which applies the reductive leaching process using organic reductant. Frequently, organic acid, sugar, biomass and agro-industrial wastes were used as reductant. Therefore, the works done by previous researchers on that particular process has been discussed. Overview on the basic principles of mathematical modelling, in regard to kinetic study (i.e., heterogeneous reaction) has also been considered. Then kinetic models that have been used to depict various leaching kinetics of reductive leaching are reviewed. In this work, Malaysian bamboo saw dust (BSD) was chosen as reductant. Consequently, some information on bamboo structure, propagation and commercial application of bamboo were described. Following this, the understanding of carbohydrates and nature of lignocelluloses; the utilization of lignocelluloses and hydrolysis of cellulose were

discuss in detailed. The understanding of this information will assist to enhance the glucose formation as well as the recovery of Mn during the leaching process. This thesis shall proceed to do so, and this literature will act as a guide to what was done in the experimental section.

## **2.2 The occurrence of Mn ore**

In many extractive efforts, geological evaluation such as the ore occurrence was the natural first step out of a chain of stages. One may need to understand the occurrence of the said ore, as the geological conditions may influence the presence of various minerals within the ore itself.

Mn is the twelfth most abundant element in the earth's crust (0.096%). Generally, most soils concentration is range from to 200 to 300 parts per million (ppm); in many rocks, concentration range from 800 to 1400 ppm and in some sedimentary rocks, its concentrations can range from 6000 to 8000 ppm (EPA, 1985). According to Fan and Yang (1999), the Mn ore deposits can divided into six types based on origin and subsequent modification: sedimentary; volcanic sedimentary; metamorphosed; hydrothermally modified; hydrothermal, and; supergene. However, most Mn ore is found as sedimentary origin, with oxide ore layers inter-bedded with iron-rich formations (Sully, 1955; Maslennikov, 2011). Mn in crystalline rock have been dissolved and re-deposited as the oxide, hydroxide or carbonate. Besides, there are some primary occurrences of Mn ore which are silicate minerals. Generally, the silicates are decomposed by water during tropical weathering.

### 2.2.1 Mineralogical assemblages and element associations

The major ores of Mn are the oxide in hydrated or dehydrated forms and to a lesser extent the silicates and carbonates (Sully, 1955; Fan and Yan, 1999). In the oxide form, the most common mode of Mn is pyrolusite, which is mainly  $MnO_2$ .  $MnO_2$  ores are formed generally due to terrestrial weathering processes and are found in a variety of environments all through the world with diverse morphology, chemistry, and physical characteristics (Das, et al., 2011).

Pyrolusite is a relatively soft grey to black colour. The pyrolusite is found as euhedral coarse grained to prismatic crystal. Its manganese content when pure is 63.2% and its specific gravity is 4.8. Another oxide form of Mn is hausmannite. It occurs as vein in igneous rock. It is brown to black in colour, hard and with a specific gravity of 4.8. The composition of hausmannite is  $Mn_3O_4$ . Psilomelane consists of hydrous manganese oxide with variable amounts of barium, aluminium and iron. Manganite, characterized as metamorphic deposits. It contains 62.4% Mn when pure and dark grey to black in colour. Most volcanic-sedimentary is dominated by 75 % of braunite which contain 62% of Mn and silica content as high as 10%. Whereas, hydrothermal deposits have various and complex mineral compositions and are mostly composed of Mn oxides and Mn silicates (Roy, 1981). The list of most common mode of Mn is tabulated in Table 2.1.

Table 2.1: The most common modes of manganese with variable elemental composition and identification (Burke and Uytendogaardt, 1985)

Mn mode and formula	Colour	Mn content (%)	Specific gravity	Miscellaneous
Pyrolusite (MnO <sub>2</sub> )	Soft grey to black	63.2 (if pure)	4.8	Coarse grained euhedral to prismatic crystal
Hausmannite (Mn <sub>3</sub> O <sub>4</sub> )	Brown to black	-	4.8	Primary origin and occurs as veins in igneous rock
Psilomelane (A <sub>3</sub> X <sub>6</sub> Mn <sub>8</sub> O <sub>16</sub> ) A: Ba, Mn, Al, Fe, Si X: (O,OH) <sub>6</sub>	Bluish grey to greyish white	45-60	3.7-4.7	Massive form
Manganite (Mn <sub>2</sub> O <sub>3</sub> .H <sub>2</sub> O)	Dark grey to black	62.4 (if pure)	4.2-4.4	Prismatic crystal or lamella crystal aggregates
Braunite (3Mn <sub>2</sub> O <sub>3</sub> .MnSiO <sub>3</sub> )	Grey with a slight brownish	62 with silica content as high 8-10	4.8	Finely granular masses

### 2.2.1(a) Pyrolusite: Relationship to manganite and Mn<sub>5</sub>O<sub>8</sub>

Pyrolusite (MnO<sub>2</sub>), a tetragonal mineral with the rutile structure, is the most stable form of manganese oxide in many terrestrial environments. Distinctions have long been recognized between the relatively rare primary form of pyrolusite and the much more common secondary form that occurs as pseudomorphic replacements of other manganese oxide minerals, particularly manganite (MnOOH); monoclinic). Secondary pyrolusite also possesses several characteristics suggestive of symmetry lower than tetragonal (Rask and Buseck, 1986). Single-crystal X ray measurements shows that the two forms of pyrolusite have identical crystal structures, primary pyrolusite is termed polianite and considered a distinct mineral. Later studies (de



Wolfl, 1959; Potter and Rossman, 1979) have found that some secondary pyrolusites are actually orthorhombic.

Ideally, pyrolusite has two equivalent lattice translations,  $a_1$  and  $a_2$ . Either of these should have an equal probability of becoming the manganite  $a$  (or  $b$ ) translation when pyrolusite is reduced to manganite. However, that is not what is observed. In the sequence manganite (primary) pyrolusite (secondary) + manganite (secondary), primary and secondary manganite invariably has the same orientations. The non-tetragonal characteristics of secondary pyrolusite have been attributed to microstructures formed in pyrolusite upon its creation from manganite (Champness, 1971). Pyrolusite and manganite have similar structures. The manganite  $a$  and  $c$  translations are halved to form  $a$  and  $c$  pyrolusite unit-cell translations, while  $b$  of manganite contracts from 5.28 Å to 4.40 Å to form the other  $a$  translation of pyrolusite (Figure 2.1). This 15% contraction along  $b$  presents the possibility that polianite microscopic cracks paralleling the manganite (010) planes separate newly made crystallites of pyrolusite.

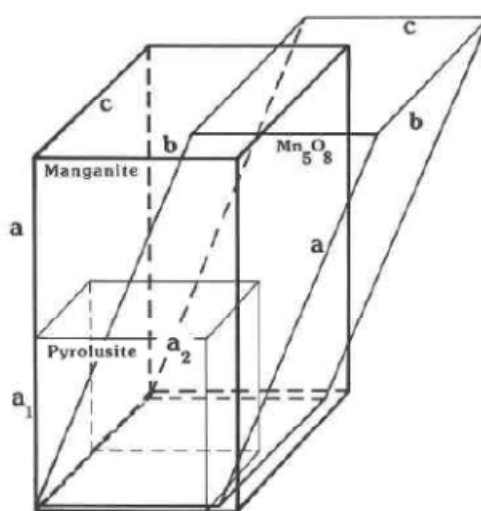


Figure 2.1: A drawing to illustrate the dimension of the pyrolusite, manganite, and  $Mn_5O_8$  unit cell and their relative orientations in the topotactic reactions (Rask and Buseck, 1986)

The unit cells of pyrolusite, manganite and Mn<sub>2</sub>O, are closely related, and in their topotactic transformations, their crystallographic axes remain in nearly the same relative orientations (Rask and Buseck, 1986). The *a*, *b*, and *c* axes of manganite correspond directly to the *a* axes and the *c* axis of pyrolusite. The *a* axis of Mn<sub>2</sub>O, is at an angle of 19° from one *a* axis of pyrolusite and *a* of manganite; *b* of Mn<sub>2</sub>O, corresponds to the *c* translation of pyrolusite and manganite; and *c* of Mn<sub>2</sub>O, has the same orientation as *b* of manganite, and *a* of pyrolusite. Pertinent crystallographic data are given in Table 2.2, and the orientation relations among the unit cells of these minerals are illustrated in Figure 2.1.

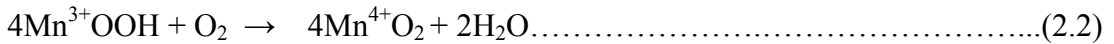
Table 2.2: Unit cell dimensions of pyrolusite, manganite, and Mn<sub>5</sub>O<sub>8</sub> (Rask and Buseck, 1986)

<b>Pyrolusite</b>	<b>Manganite</b>	<b>Mn<sub>5</sub>O<sub>8</sub></b>
a: 4.3999 Å° b: 2.8740 Å°	a: 8.98 Å° b: 5.28 Å° c: 5.71 Å° β: 90°	a:10.347 Å° b: 5.72 Å° c: 4.852 Å° β: 109°25′

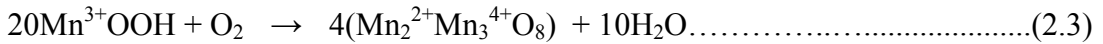
The phase transformations of manganite upon heating in air show an interesting features in that Mn is first oxidized in the MnOOH to MnO<sub>2</sub> transition but upon further heating, Mn is reduced as MnO<sub>2</sub> goes to Mn<sub>2</sub>O<sub>3</sub> and finally to Mn<sub>3</sub>O<sub>4</sub>. This growth of Mn<sub>5</sub>O<sub>8</sub> from pyrolusite confirms the finding that in air at temperature above 300°C, Mn<sub>5</sub>O<sub>8</sub> form from secondary pyrolusite, not from manganite. The reaction of pyrolusite to Mn<sub>5</sub>O<sub>8</sub> can be written as



The reaction of manganite to pyrolusite may be written as



The most likely mechanism for this reaction is migration of H out of manganite, rather than O influx into manganite. However, in the absence of mechanistic evidence, we have chosen to write this oxidation reaction in the more conventional manner. The finding of low-temperature Mn<sub>5</sub>O<sub>8</sub>-pyrolusite intergrowths in close proximity to manganite suggests that Mn<sub>2</sub>O<sub>3</sub> may also be formed from manganite decomposition by a reaction such as



Equation 2.2 and 2.3 may operate simultaneously, the proportion of pyrolusite to Mn<sub>2</sub>O<sub>3</sub>, depending on local variations in oxygen fugacity. Crystallite size is a further factor in controlling such reactions; for the oxidation α-MnOOH (groutite). The microspores' that develop parallel to manganite (010) as a result of these reactions may provide channels for the escape of H<sub>2</sub>O. They may also facilitate migration of oxygen into the crystal and thus oxidation and elimination of Mn<sub>5</sub>O<sub>8</sub>, by the reverse of Equation 2.1.

2.2.1(b) Significant mineral in LGMO- Al-substituted Goethite (Fe<sub>0.93</sub>Al<sub>0.07</sub>) OOH

Manganese mineralization in the soft iron ore has taken place both in goethitized iron ore and in the argillized wall rock. The manganese oxides are found as vein in the soft iron ore, as impregnations in the argillized wall rock and in secondary calcite veins. This manganese mineralization is mainly concentrated to the border zone between the soft iron and the argillized skarn and leptite rocks. The quite predominating manganese oxide mineral in these veins is pyrolusite. The

remarkably low content of some of the trace elements in the pyrolusite and the todorokite may be explained through the conditions under which these minerals were formed. These veins cut both the soft iron ore and the argillized wall-rock; this indicates that they were formed during a late phase of the alterations. The physical condition of the argillized rocks and of the soft iron ore bodies prevented any further considerable transport of water which could carry suitable cations to the manganese oxide. It is a well-known fact that manganese oxides strongly absorb certain cations, amongst them those given in the above spectrochemical analyses (Ljunggren, 1960).

The ionic substitution of aluminium for iron in goethite is well documented and has been shown to occur in goethite from soils. Al substitution ranges from zero to about 33% mol. Schulze (1984) showed that the amount of Al substitution may be an indicator of past or present pedogenic conditions. The  $\text{Al}^{3+}$  ion is slightly smaller than the  $\text{Fe}^{3+}$  ion,  $0.53\text{\AA}$  vs.  $0.65\text{\AA}$  thus, when Al substitutes for Fe in the goethite structure, the average size of unit cell decreases. The structure of goethite ( $\alpha$ - $\text{FeOOH}$ ) and isostructural diasphore ( $\alpha$ - $\text{AlOOH}$ ) is based on the hexagonal close packing of oxygen atoms with 6-fold coordinated metal atoms occupying octahedral positions. The metal atoms are arranged in double rows to form what can be described as doubled chains of octahedra which run the length of the  $c$  axis (Schulze, 1984).

Early studies on dissolution of goethite dealt with mechanism of dissolution and effect of crystal morphology on dissolution. There could be varying degrees of substitution of Al for goethite-Fe in terrestrial weathering environments,  $\text{Fe}_{1-x}\text{Al}_x\text{OOH}$  (where  $x < 1.0$ ). The level of substitution alters crystal size, texture surface

area, morphology and other structural properties that influence the rates and mechanisms of goethite dissolution. The extent of co-existing ions in the outer or inner sphere of goethite crystallography may enhance or inhibit the release of Fe (III) into solution in acid medium.

Aluminium incorporated in the structure does not only reduce the unit cell size, because it is a smaller cation, but also influence the crystal size and thereby the surface area (Schulze, 1984). This indicates that as well as having a direct and specific effect on the structure, Al also influences other goethite properties. This is because Al modifies the crystallization conditions, and thus crystal growth rate and, in turn, crystal size, morphology and degree of order. All these effects are not specific to Al but may be caused by any other component interfering with crystal growth (Schwertmann, 1983).

### 2.2.2 Classification of manganese ore

Mn ores exhibit a wide variability in composition, particularly in the balance of the manganese and iron content. 95% of the total manganese ore which is mined is used for metallurgical purposes, the ores is classified on the basis of the manganese content and the type of ferro-alloy for the manufacture of which they are to be used. The metallurgical classifications are as follows; i) manganese ore containing more than 35% manganese which are suitable for the manufacture of high or low grade ferromanganese; ii) Ferruginous manganese ore or spiegel ores containing 10-35% percent manganese which are used for the manufacture if spiegeleisen; and iii) manganiferrous iron ores, containing 5-10% manganese are used for the manufacture of manganiferrous pig iron (Sully, 1995).

### 2.2.3 Impurities in Manganese

Common impurities in Mn ores are metallic impurities, gangue composition, volatile matter and other miscellaneous impurities. These impurities may impart undesirable production of Mn. The most common metallic impurities are iron, whilst others are lead, zinc, silver, tungsten, nickel and copper. With the exception of zinc, these impurities are reduced during smelting and are retained in the metal. Zinc is volatilized during smelting and may hinder furnace operation. However, in order to be suitable for the production of ferromanganese the proper ratio of manganese to iron in the ore must be nine to one. Therefore, iron which is present as oxide in manganese ore cannot readily be removed (Sully, 1955). Beside that, iron is also an undesirable impurity if the Mn ore is to be used for battery production (Das et al., 2011) or for decolorizing glass (EPA, 1985).

The gangue impurities are slag-forming. A certain quantity of slag is valuable in metallurgical operation but the quantity must not be excessive. The volatiles impurities are driven off in blast furnace operation of manganese alloy. Carbonate ore such as rhodocrosite decompose to form volatile carbon dioxide. However, it can be effectively removed prior calcinations (Sully, 1955). Finally, phosphorus and sulphur are miscellaneous impurities in Mn ore. In the steel making process, the nature of phosphorous in the ore cannot be removed by ore dressing methods but can be removed during smelting by applying low temperature in electrical furnace. However, sulphur removal is favour in higher temperature. Therefore, the current attention being directed to control phosphorous and sulphur by performing two stage refining process in electrical furnace. As a result, the quality of steel produced is under permissible phosphorus and sulphur content (Smaier, 1983).

### 2.3 Application of manganese ore

The principal use of Mn is in the metallurgical industries primarily in the steel making in the form of manganese ferro-alloy. In steelmaking, Mn performs vital function as deoxidizer and desulphurizer since no quality steel can be produced without the addition of manganese. When Mn added to the steel, Mn act as deoxidant by reducing iron oxide and combining with free O<sub>2</sub>. Thus, it will produce the clean ingot (Sully, 1955). Besides that, by adding Mn in steel, it will react with sulphur and retains it as manganous sulphide (MnS). It also gives alloying properties of steel such as strength, toughness, hardness, and hardenability (EPA, 1985). Relatively small quantities of Mn are used for alloying with nonferrous metals, such as copper-manganese alloy, aluminium alloy and Mn bronzes. Mn imparts corrosion resistance in copper-manganese alloy and Mn bronze. While in aluminium alloy, Mn imparts strength, hardness and stiffness. For example copper manganese alloy are used for turbine blades; Mn bronze for propellers and aluminium alloy in manufacturing of beverage cans (Sully, 1955; EPA, 1985 and Corathers, 2010).

As well as in metallurgical industries, Mn in oxide form is important in non-metallurgical application such as in electrical and dry cell batteries; glass making; ceramic industry; paint and varnish industry. High grade of pyrolusite is required for manufacturing of electrical batteries. The manganese oxide (MnO<sub>2</sub>) acts as depolarizer in the electrical cells (Sully, 1955). In glass making, iron is common impurity in the sand used. When iron is converted to ferrous silicate, it gives a green coloration to the glass. In order to combat the iron effect, the addition of native Mn ores can removed this coloration and produced a high quality of glass (Sully, 1955 and EPA, 1985). In the ceramic industry, MnO<sub>2</sub> is used to produce brown, purple and

black glaze as well as slate coloured in tiles and bricks (Sully, 1955 and Das et al., 2011).  $\text{MnO}_2$  have an appreciable field of application in the paint and varnish industry where it is used as oil driers by absorption of  $\text{O}_2$  by the oils (Sully, 1955; Corathers, 2012).

$\text{MnO}_2$  is also extensively used in the manufacture of chemical especially in manufacturing of electrolytic manganese dioxide (EMD) and chemical manganese dioxide (CMD). Generally, EMD is produced by pyro-hydrometallurgical process, while CMD is produced by thermal decomposition process. The produced EMD and CMD are normally used in alkaline batteries (EPA, 1985 and Zhang and Cheng, 2007). Some other chemical produced is organic compound which is able to use as fertilizer in agriculture field. The Mn has been shown to be important feed additives for plant nutrition. While in agriculture field, Mn compound act as feed additives in plant nutrition.

#### **2.4 Production and consumption of Mn ores; steel production and, domestic price**

In the present scenario, the demand for Mn ore has increased due to increase in the manufacture of steel over the years. This has led the price to rise for both Mn ores and steel. The world production of Mn ore is shown in Table 2.3 from 2006 to 2010. Attention has already been drawn to the close correspondence between Mn



Table 2.3: Summary of world production of manganese ore, ferromanganese and silicomanganese and U.S manganese consumption between 2006 to 2010 (Corathers, 2008; 2009; 2010; 2011; 2012)

<b>Production, consumption and prices</b>	<b>2006 Minerals Year Book</b>	<b>2007 Minerals Year Book</b>	<b>2008 Minerals Year Book</b>	<b>2009 Minerals Year Book</b>	<b>2010 Minerals Year Book</b>
World production of manganese ore.	Rose by 7% on gross weight basis and 8% content weight basis compared in 2005.	Rose by 9% on gross weight basis and 3% on a content weight basis compared in 2006.	Rose by 8% on a gross weight basis and by 6% on a content-weight basis compared in 2007.	Decreased by 12% on gross weight basis and 16% content weight basis compared in 2008.	Increased by 26% on a gross-weight basis and by 31% on a contained weight basis, compared with that in 2009.
Leading producer of manganese ore.	Gross weight basis - China; content weight basis- South Africa.	Gross weight basis - China; content weight basis- South Africa.	Gross weight basis - China; content weight basis- South Africa.	Gross weight basis and content weight basis- China.	Gross weight basis and content weight basis- China.
World production of ferromanganese and silicomanganese	Rose by 14% on gross weight basis compared with the revised amount in 2007.	Rose by 5% on gross weight basis compared with the revised amount in 2007.	Fell slightly to 13.2 million mt on a gross weight basis compared with the revised amount in 2007.	Decreased by 8% to 12.5 million mt on a gross weight basis compared with the revised amount in 2008.	Increased by 16% to 15.2 million mt on a gross-weight basis compared with the revised amount in 2009.
Leading producer of ferromanganese and silicomanganese	China	China	China	China	China
U.S manganese consumption	1.05 million mt, 36% increased from 773, 000 mt in 2005.	1.03 million mt, 2% decreased from 1.05 million mt in 2005.	868,000 mt, an 11% decrease from the revised amount of 975,000 mt in 2007.	445, 000 mt, 47% decreased from revised amount of 844, 000 mt in 2008.	758,000 mt, a 68% increase from the revised amount of 451,000 mt in 2009.
Average domestic price -Metallurgical grade ore -Ferroalloy	48% manganese to be about \$3.51 per mt	48% manganese to be about \$3.48 per mt	48% manganese to be at \$12.15 per mt	48% manganese was \$6.61 per mt.	46% to 48% manganese was \$9.18 per mt.

ore production and steel production (e.g., ferromanganese and silicomanganese). The price of Mn ores throughout the period is continuing seen to be increasing in lines with demand.

World production of Mn ore in 2010 rose by 26% on a gross weight basis, and by 31% on a contained-weight basis, compared to that in 2009 (Corathers, 2012). Nonetheless, the current worldwide Mn production is still unable to cope with the demand from the growing metallurgical industry. It is reported that metallurgical applications of manganese consume 77% to 90% of the total Mn ore production (Corathers, 2012). Throughout the period of 2006 to 2010, China was the leading producer of Mn ores on gross-weight basis. South Africa is leading the Mn production on content-weight basis in the period of 2006 to 2008.

World steel production (e.g., ferromanganese and silicomanganese) increased by 16% to 15.2 metric ton (mt) on a gross-weight basis compared with the revised amount in 2009. China was the largest producer of this steel making. There were significant increases in annual average of ferromanganese and silicomanganese prices in 2010 from those in 2006, 2007 and, 2009 because of improved global economic conditions. The United State Geological Survey estimated the annual United State average contract price of metallurgical-grade ore containing 46% to 48% manganese was \$9.18 mt for 2010.

As reported in Mineral Commodity and Summaries (2012), no satisfactory substitute exists for replacing Mn by other metals in its most major applications. As number of products from Mn applications continues to rise, the Mn demand